HEAVY-ION RESULTS FROM CMS*

Artur Kalinowski

on behalf of the CMS Collaboration

Faculty of Physics, University of Warsaw
Pasteura 5, 02-093 Warsaw, Poland

Received 31 March 2025, accepted 14 May 2025, published online 26 June 2025

The Compact Muon Solenoid detector (CMS) was designed to analyze data mainly from proton–proton collision, but its robust design allows also for the analysis of data from heavy-ion collisions. This contribution describes a few examples of recent results of heavy-ion data analyses from CMS.

DOI:10.5506/APhysPolBSupp.18.5-A12

1. Introduction

The Compact Muon Solenoid [1] is one of two general-purpose detectors operating at the LHC [2]. The universal design of the apparatus allows for analyses of large variety data including heavy-ion, proton–ion, proton–proton, and photon–photon collisions. Central ion–ion collisions provide a unique laboratory for studies of dense, colored matter — the Quark–Gluon Plasma (QGP). Ultraperipheral collisions, where the colliding objects are separated by a distance greater than the sum of their radii, provide environment for studies of photon–photon interactions. The analyses described in this contribution are based on the data from 1.7 nb^{-1} of proton–proton reference runs from 2017 and 302 pb^{-1} of lead–lead (PbPb) data from 2018, both collected at 5.02 TeV nucleon–nucleon center-of-mass energy.

2. Study of QGP impact on b-quark hadronization

Various probes are used to study QGP properties, among which are b quarks. The presence of the colored medium affects the hadronization of the b quarks as b quarks lose energy via scattering and QGP-induced radiation. Comparison of B meson p_{T} spectra measured in proton–proton

* Presented at the 31st Cracow Epiphany Conference on the *Recent LHC Results*, Kraków, Poland, 13–17 January, 2025.

and heavy-ion collisions can be used to constrain QGP models [3]. The nuclear modification factor is defined as

$$R_{AA}(p_{\mathrm{T}}) = \frac{1}{T_{AA}} \frac{\mathrm{d}N^{B^+,B_s^0}_{\mathrm{PbPb}}}{\mathrm{d}\,p_{\mathrm{T}}} \Bigg/ \frac{\mathrm{d}N^{B^+,B_s^0}_{pp}}{\mathrm{d}\,p_{\mathrm{T}}}, \tag{1}$$

where T_{AA} corresponds to the parton–parton luminosity in heavy-ion collisions. The B mesons are identified via $B \to J/\psi + X$ and $J/\psi \to \mu^+\mu^-$ decays, with X representing $K^{\pm}$ for B^+ and $\phi(1200)$ in the case of B_s^0 mesons, respectively. The $\phi(1200)$ is reconstructed via $\phi(1200) \to K^+K^-$. Since the CMS detector lacks hadron identification, charged tracks are assumed to be kaon candidates, and the invariant mass closest to the target particle (B or $\phi(1200)$) is selected.

Figure 1 shows the invariant mass distributions for the B^+ (left) and B_s^0 (right) in pp data. Similar distributions are obtained for the PbPb data. The extracted signal yields are used to calculate R_{AA} in p_{T} bins. The measured R_{AA} is shown in figure 2 together with predictions from different models.

The experimental uncertainties are smaller than those of the CUJET3.0 and AdS/CFT HH, enabling constraints on parameters such as the parton-medium coupling D in the AdS/CFT HH framework [4, 5].

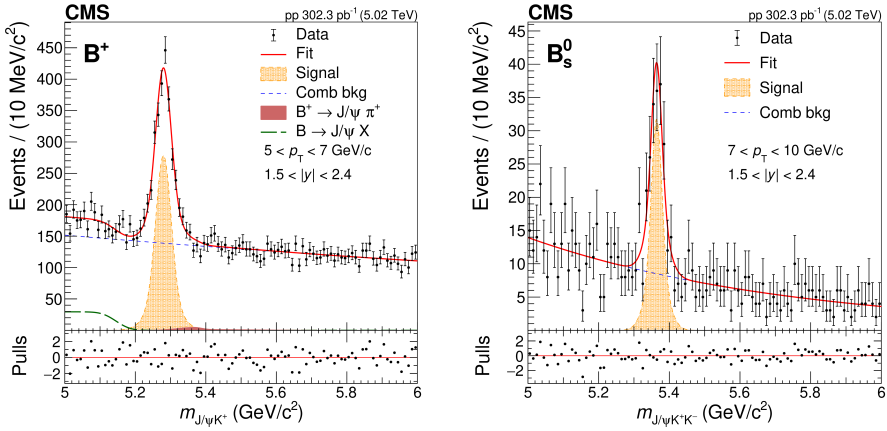

Fig. 1. Invariant mass of the $\mu\mu K$ (left) and $\mu\mu KK$ (right) systems. Event counts in data are shown with markers, while the background estimation is shown with a solid line. The signal estimate from B^+ (left) and B_s^0 (right) is shown as a full histogram [3].

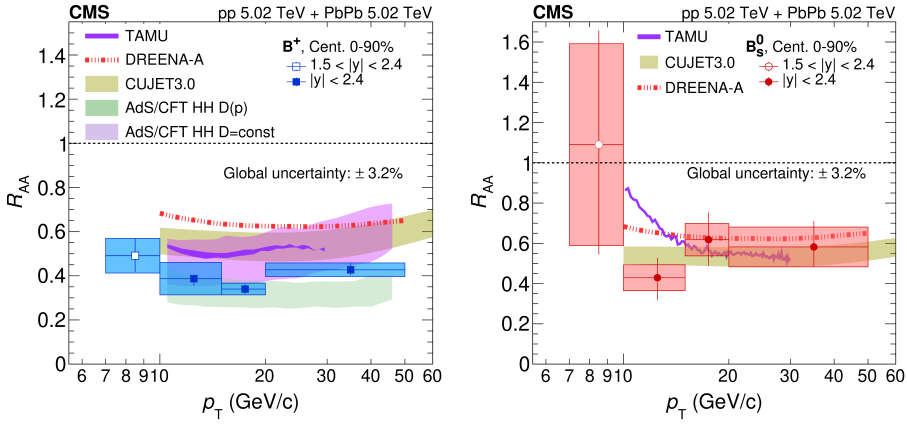

Fig. 2. The p_{T} dependence of the nuclear modification factor for B^{+} (left) and B_s^0 (right) mesons. The data points are shown with markers, while the model predictions are shown with lines [3].

3. Study on QGP medium response to hard probes

The CMS Collaboration performed the first measurement of low-p_{T} charged hadron distributions (in pseudorapidity and azimuthal angle) relative to Z bosons in PbPb collisions [6].

While the QGP affects colored objects, the medium itself responds to these probes. QGP response can be experimentally accessed by the study of the low transverse momentum particles produced in the collision. A process where a Z boson is produced in association with a high transverse momentum parton was used to study this effect. The Z boson, which is not affected by the QGP, can be used as a proxy of the initial parton energy and momentum. The azimuthal angle distributions relative to the Z boson direction are therefore sensitive to the QGP response to the parton created in the initial hard scattering.

The associated yield is defined as

$$\frac{1}{N_Z}\Delta N_{\mathrm{ch}}\left(\Delta\phi_{\mathrm{ch},Z},\Delta y_{\mathrm{ch},Z}\right)=\frac{N_{\mathrm{ch}}(\Delta\phi_{\mathrm{ch},Z},\Delta y_{\mathrm{ch},Z})-\langle N_{\mathrm{ch}}\rangle}{N_Z}\,, \qquad (2)$$

where N_Z is the number of Z bosons, $N_{\mathrm{ch}}(\Delta\phi_{\mathrm{ch},Z},\Delta y_{\mathrm{ch},Z})$ is a number of charged hadrons in $(\Delta\phi_{\mathrm{ch},Z},\Delta y_{\mathrm{ch},Z})$ bin. The $\langle N_{\mathrm{ch}}\rangle$ is the average over the distribution. Such representation removes the contribution from the charged particles from multi-parton interactions. Figure 3 shows the normalized associated yield for the central PbPb collisions and the difference between PbPb and pp yields. A clear difference between the PbPb and pp data is visible for charged particles in the lowest p_{T} range. A number of model

predictions were compared with the data. A deficit in the charged-particle yield in the region of $\Delta\phi_{\mathrm{ch},Z} = 0$ can be associated with a negative medium wake, while an excess at $\Delta\phi_{\mathrm{ch},Z} = \pi$ can be explained by medium-induced radiation and momentum-broadening effects. PYTHIA 8 predictions (without QGP effects) disagree with the data, highlighting the need for refined models [7, 8].

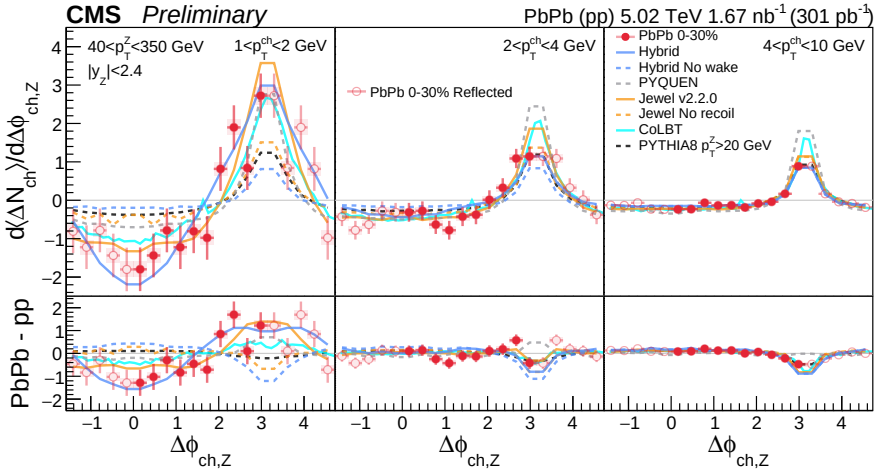

Fig. 3. The measured normalized associated yield for events with Z boson $p_{\mathrm{T}} > 40$ GeV in the central PbPb collisions. The data points are shown with markers, while the model predictions are shown with lines. The lower panel shows the difference between the yields in the PbPb and pp yields. The vertical bars and shaded boxes represent the statistical and systematic uncertainties, respectively [6].

4. Study of light-by-light scattering

Ultraperipheral PbPb collisions provide a unique environment for studying light-by-light (LbL) scattering. Ultraperipheral collisions can be studied in collisions of any type of beams, but in the case of heavy ions, one can profit from a Z^4 enhancement of the photon beam luminosity with respect to the proton–proton case [10].

The effective energy of the beam is of the order of $E_{\gamma\gamma} \approx 100$ GeV, while the $\gamma\gamma$ luminosity is about 10^7 times larger than in the case of the proton–proton [9]. This allows for measurements of extremely rare LbL scattering process. Measurement of such a rare process might reveal, possibly relatively large, contribution from the physics beyond Standard Model. In the case of LbL, one might expect contribution from axion-like particles exchanged in the s channel.

The CMS Collaboration analyzed 1.65 fb^{-1} of PbPb data collected in 2018 to search for the LbL scattering and the Breit–Wheeler ($\gamma\gamma \to e^+e^-$) processes [11]. In this analysis, the Breit–Wheeler process was used as the control process. Figure 4 presents schematic diagrams for the main contributions to the final states: signal — light-by-light scattering, main background — central exclusive diphoton production, control process — Breit–Wheeler process, and finally, the axion-like particle exchange. The Breit–Wheeler

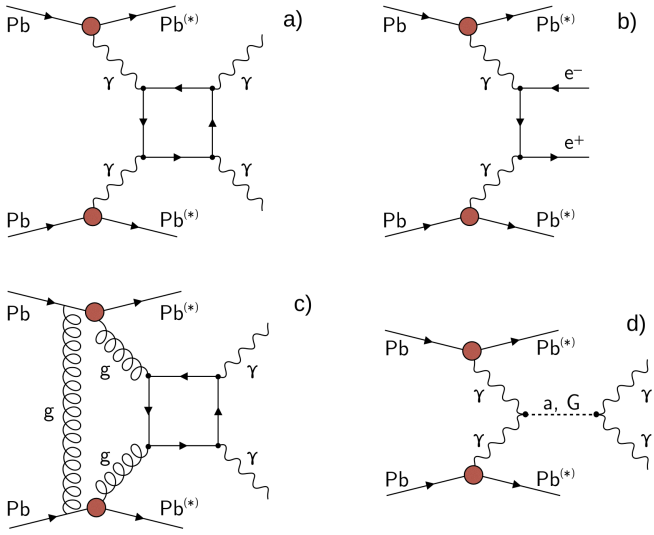

Fig. 4. Schematic diagrams for the main processes contributing to the final states considered in the LbL scattering analysis. The light-by-light scattering (a), the Breit–Wheeler process (b), central exclusive diphoton production (c), and the axion-like particle exchange (d) [11].

process (Fig. 4 (b)) was very clean with virtually no background. The cross section for both the Breit–Wheeler and LbL processes were measured in the fiducial phase space defined by the analysis selection criteria: $E_{e/\gamma} > 2$ GeV, $|\eta_{e/\gamma}| < 2.2$, $p_{\mathrm{T}}^{e/\gamma} < 1$ GeV, $m_{ee/\gamma\gamma} > 5$ GeV, and $(1 - \Delta\varphi_{\gamma\gamma,ee}/)\pi < 0.01$. Figure 5 shows the measured fiducial $\gamma\gamma \to e^+e^-$ cross section as a function of the e^+e^- system invariant mass. The experimental result is in a very good agreement with the theoretical prediction. Once the control process was well established, the differential cross section for the LbL scattering was measured. Figure 6 presents a comparison of the measured fiducial cross section with the theoretical prediction. The experimental result is in a good agreement (within large uncertainties) with model predictions. The axion-like particles exchange in the s channel would be visible as a peak in the

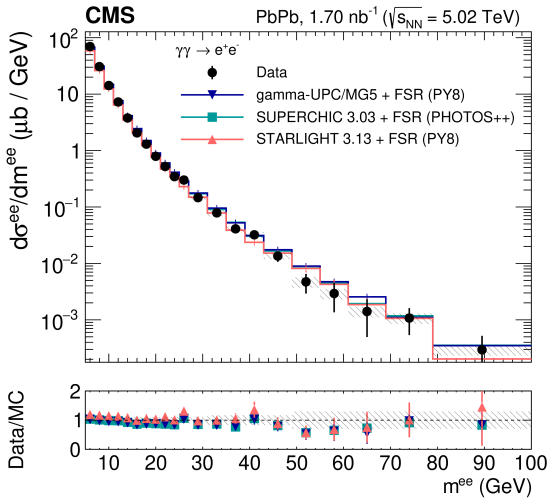

Fig. 5. Differential cross section for the Breit–Wheeler process reported for the fiducial phase space defined in the text. Vertical bars (hatched bands) show statistical (systematic) uncertainties [11].

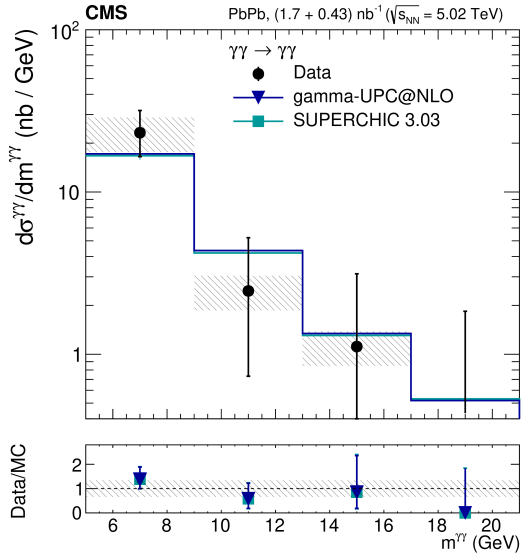

Fig. 6. Differential cross section for the $\gamma\gamma \to \gamma\gamma$ process reported for the fiducial phase space defined in the text. Vertical bars (hatched bands) show statistical (systematic) uncertainties [11].

invariant mass distribution of the $\gamma\gamma$ system. Figure 7 (left) presents data points overlaid on the expected axion signals for $m_a = 14$ and 20 GeV/c^2. As no excess over the Standard Model prediction was observed, exclusion limits on the axion-like production cross section were calculated. The exclusion limits as a function of the axion mass are shown in Fig. 7 (right).

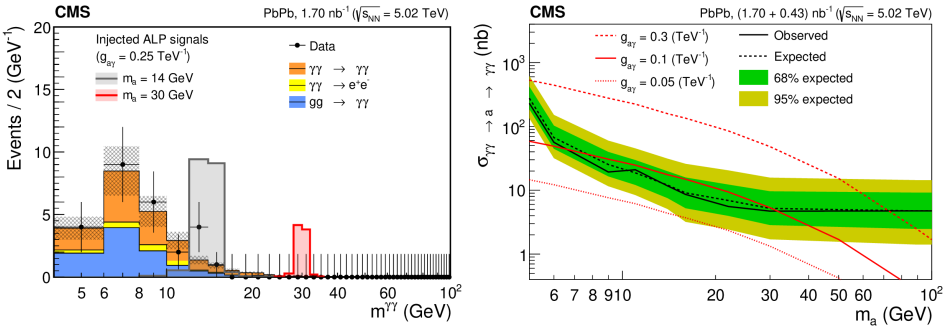

Fig. 7. Left panel: invariant mass of the $\gamma\gamma$ system measured in the $\gamma\gamma \rightarrow \gamma\gamma$ process. The data points are shown with markers, while the expected Standard Model and axion-like contributions are shown as full histograms. Right panel: the exclusion limit on the axion-like production cross section as a function of the axion mass [11].

5. Conclusions

Central and ultraperipheral heavy-ion and proton–ion collisions provide a unique opportunity for both QCD, and QED studies. The CMS Collaboration performed a number of analyses of the heavy-ion data which improves our understanding of the complicated structure of low-momentum, many-body QCD. An exhaustive summary of the observations collected so far is given in a recent review of the CMS heavy-ion results [12].

This research was partially funded by the Ministry of Science and Higher Education, Poland grant 2022/WK/14.

REFERENCES

[1] CMS Collaboration (S. Chatrchyan *et al.*), *J. Instrum.* **3**, S08004 (2008).

[2] L. Evans, P. Bryant, *J. Instrum.* **3**, S08001 (2008).

[3] CMS Collaboration (A. Hayrapetyan *et al.*), *J. High Energy Phys.* **2025**, 195 (2025), arXiv:2409.07258 [nucl-ex].

[4] M. Rohrmoser, P.-B. Gossiaux, T. Gousset, J. Aichelin, *J. Phys.: Conf. Ser.* **779**, 012032 (2017), arXiv:1611.01854 [hep-ph].

[5] S. Cao, G.Y. Qin, S.A. Bass, *Nucl. Phys. A* **931**, 569 (2014), arXiv:1408.0503 [nucl-th].

[6] CMS Collaboration (A. Hayrapetyan *et al.*), CMS-PAS-HIN-23-006.

[7] W. Chen *et al.*, *Phys. Rev. Lett.* **127**, 082301 (2021).

[8] Z. Yang *et al.*, *Phys. Rev. Lett.* **130**, 052301 (2023).

[9] V.M. Budnev, I.F. Ginzburg, G.V. Meledin, V.G. Serbo, *Phys. Rep.* **15**, 181 (1975).

[10] A.J. Baltz *et al.*, *Phys. Rep.* **458**, 1 (2008), arXiv:0706.3356 [nucl-ex].

[11] CMS Collaboration (A. Hayrapetyan *et al.*), CMS-PAS-HIN-21-015.

[12] CMS Collaboration (A. Hayrapetyan *et al.*), *Phys. Rep.* **1115**, 219 (2025), arXiv:2405.10785 [nucl-ex].